Research in Astron. Astrophys. **2011** Vol. **11** No. **10**, 1171–1184
http://www.raa-journal.org *http://www.iop.org/journals/raa*

Research in Astronomy and Astrophysics

Serendipitous discovery of warm absorbers in the Seyfert 2 galaxy IRAS 18325–5926 *

Shui-Nai Zhang[1,2], Qiu-Sheng Gu[1,2], Li Ji[3] and Zhi-Xin Peng[1,2]

[1] Department of Astronomy, Nanjing University, Nanjing 210093, China; *snzhang@nju.edu.cn*
[2] Key Laboratory of Modern Astronomy and Astrophysics, Nanjing University, Ministry of Education, Nanjing 210093, China
[3] Key Laboratory of Dark Matter and Space Astronomy, Purple Mountain Observatory, Chinese Academy of Sciences, Nanjing 210008, China

Received 2010 September 3; accepted 2011 May 4

Abstract Warm absorption is a common phenomenon in Seyfert 1s and quasars, but is rare in Seyfert 2s. We report the detection of warm absorbers with high energy resolution in the Seyfert 2 galaxy IRAS 18325–5926 for the first time with *Chandra* HETGS spectra. An intrinsic absorbing line system with an outflow velocity ~ 400 km s^{-1} was found, which is contributed by two warm absorbers with FWHM of 570 km s^{-1} and 1360 km s^{-1}, respectively. The two absorbers were adjacent, and moving transversely across our line of sight. We constrained the distance between the center and the absorbers to be a small value, suggesting that the absorbers may originate from the highly ionized accretion disk wind ejected five years ago. The perspective of this type 2 Seyfert provides the best situation in which to investigate the vertical part of the funnel-like outflows. Another weak absorbing line system with zero redshift was also detected, which could be due to Galactic absorption with very high temperature or an intrinsic outflow with a very high velocity ~ 6000 km s^{-1}.

Key words: galaxies: Seyfert — galaxies: absorption lines — X-rays: galaxies — galaxies: individual: IRAS 18325–5926

1 INTRODUCTION

A warm absorber (WA) in the X-ray band was firstly found by Halpern (1984) using the *Einstein* telescope and has been studied extensively since then. These types of ionized absorbing gas exist in about 50% of Seyfert 1s (Reynolds 1997; George et al. 1998) and quasars (Piconcelli et al. 2005; Misawa et al. 2007; Ganguly & Brotherton 2008), characterized by X-ray absorption lines which are usually blue-shifted by a few hundred km s^{-1}. As a consequence, WAs are considered as a potential form of active galactic nuclei (AGNs) feedback. The fundamental question is how WAs originate and where they are located. The proposed models include accretion disk wind (Elvis 2000), clouds in the broad line region (BLR) (Risaliti & Elvis 2010) or the narrow line region (NLR) (Kinkhabwala et al. 2002), winds from the putative obscuring torus (Krolik & Kriss 2001) and a shocked outflow (Pounds & Vaughan 2011), which span a wide range in radial distances from the central ionizing

* Supported by the National Natural Science Foundation of China.

source. However, different models may predict similar spectra, e.g. NGC 3783 (Netzer et al. 2003 versus Krongold et al. 2005) and NGC 4051(Krongold et al. 2007 versus Steenbrugge et al. 2009). Determination of the origin of WAs is still mired in ambiguity.

In Seyfert 2s, the direct view to the continuum source is blocked by the molecular torus and the spectrum is featured in emission lines instead of warm absorptions (Sako et al. 2002). Only a few possible absorption features have been reported in Seyfert 2s, such as NGC 3786 (Komossa & Fink 1997) and NGC 4507 (Comastri et al. 1998; Matt et al. 2004). In this work, we searched through all type 2 AGNs in the archive of the *Chandra* High Energy Transmission Grating Spectrometer (HETGS) observations and focused specifically on investigating WAs in a serendipitous Seyfert 2 galaxy IRAS 18325–5926. It has been observed with several early X-ray telescopes, such as *RXTE*, *BeppoSAX* and *XMM-Newton*, but none of them recorded the ionized absorption (Iwasawa et al. 2004). The luminosity distance of IRAS 18325–5926 is 81.1 Mpc based on the optical spectroscopic redshift 0.020 (Jones et al. 2004). We adopt a cosmology of $H_0 = 73\ \mathrm{km\ s^{-1}\ Mpc^{-1}}$ throughout this paper.

This paper is organized as follows. In Section 2, we describe the data reduction. Section 3 is devoted to the analysis of the data and Section 4 to the detailed model of the ionized absorbers of IRAS 18325–5926. In Section 5 we discuss our results and we draw our conclusions in Section 6.

2 OBSERVATIONS AND DATA REDUCTION

2.1 Data Reduction

Two observations of IRAS 18325–5926 were performed with the *Chandra* HETGS (Canizares et al. 2005) in 2002 March (PI Canizares) with a total exposure time of 108 ks over three days (Table 1). Data were reduced uniformly and in a standard way (Zhang et al. 2011) using the *Chandra* Interactive Analysis of Observations (CIAO) software (Version 4.2) and the *Chandra* Calibration Database (Version 4.3.0). All measurements in the paper were obtained from the combined first-order spectra from both the High Energy Gratings (HEG) and the Medium Energy Gratings (MEG) instruments. The statistical errors in the line energies are typically small and likely dominated by instrument uncertainties. The relative wavelength accuracy of the HEG is 0.0010 Å and that of the MEG is 0.0020 Å. The spectral analysis was carried out using the Interactive Spectral Interpretation System (ISIS version 1.6.3, Houck 2002). We adopted C-statistics (Cash 1976) to find the best-fitting model parameters and the 90% confidence for the quoted errors.

Table 1 *Chandra* HETGS Observation Log

ID	Start time	Exposure time (ks)
3148	2002.03.20 11:46:45	56.9
3452	2002.03.23 16:11:16	51.1

2.2 The Variations

Figure 1 shows the count rate of the short wavelength band (1.5–12 Å) as a function of time for the two observations of IRAS 18325–5926, binned in intervals of 400 s. The strong variations over a relatively short time scale are illustrated in the light curves. The count rate varies from the minimum of 0.2 to the maximum of 0.6 during the observations. We prepared two subsets of data according to the variation.

Our first group of data is comprised of observations of ID 3148 and ID 3452. There is a 50% change in the mean count rate between ID 3148 (0.3 counts per second) and ID 3452 (0.45 counts per second), that is separated by three days. The large amplitude and the quick variability of the

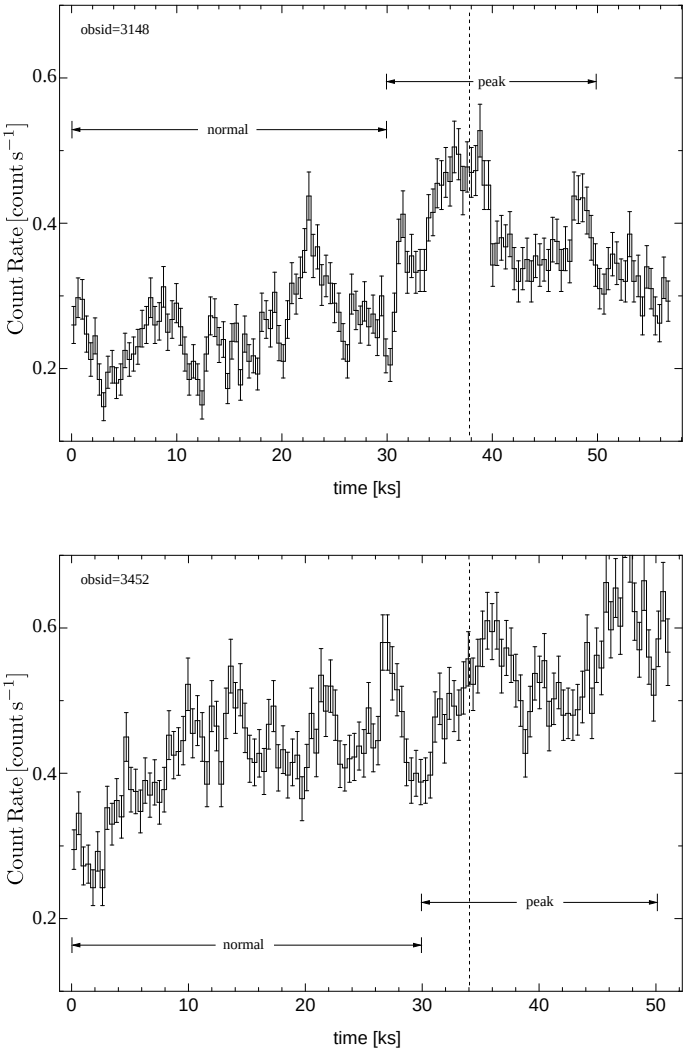

Fig. 1 IRAS 18325–5926's X-ray light curves. The dashed lines indicate two peaks, between which are five periodicities. The "normal" interval is 30 ks in each observation, while the "peak" interval is 20 ks.

ionizing luminosity is helpful for determining the location of WAs, because one key diagnostic is based on applying non-equilibrium models to the time varying AGNs (Nicastro et al. 1999).

Our second group of data is divided into "normal" and "peak" sections, defined by the following strategy. We denoted the peaks of ID 3148 (0.5 counts per second) and ID 3452 (0.6 counts per second) with dashed lines in Figure 1 and then denoted the "peak" interval (20 ks around the dashed line, and "normal" interval (30 ks before the "peak" interval). The "peak" intervals of the two observations are combined, as are the "normal" intervals. The mean count rate increased by a factor of 1.5 from "normal" to "peak." A 58 ks periodicity of IRAS 18325–5926 was found in both a 5-day *ASCA* observation (Iwasawa et al. 1998) and a combined 5-day set of *RXTE* observations (Fabian

et al. 1998). The time interval between the two peaks of our light curves is 290 ks, which happened to be five cycles, though the periodicity was not evident. One of the potential mechanisms for the periodicity is an object orbiting the black hole (BH) (Iwasawa et al. 1998). Since this object could be the origin of WAs (e.g. the extension of a star), it is necessary to estimate the response in the opacity of WAs with respect to the ionizing luminosity during a period. "Normal" and "peak" correspond to the phases where the object is moving beside and behind the BH, respectively.

3 SPECTRAL ANALYSIS

3.1 Fitting the Continuum

The IRAS 18325–5926 spectrum is affected by a relatively low Galactic absorption: $N_{\rm H} = 6.41 \times 10^{20}\,{\rm cm}^{-2}$ (Kalberla et al. 2005), which is included in the following analysis. Since the soft X-ray band longer than 12 Å was heavily absorbed, we fitted the spectrum in the 1.5–12 Å band using a 0.005 Å wide bin. All spectra were well fitted by an absorbed power-law except for small residuals between 9.5 – 10 Å (Fig. 2). However, adding a thermal or a non-thermal component to the power-law continuum did not improve the fitting statistics.

Table 2 presents the values for the best continuum fit, indicating that the 2–10 keV flux of both groups of data increased by a factor of 1.5. Neither the spectral slope nor the column density experienced significant variations. The intrinsic neutral absorption is slightly under $10^{22}\,{\rm cm}^{-2}$, which is usually the dividing line between type 1 and type 2 AGNs. The variation of the absorbing column density is common for Serfert 2s, the time scale of which usually lasts for years (Risaliti et al. 2002) and several Seyfert 2s have been observed switching from Compton-thin to reflection-dominated cases or vice versa (Matt et al. 2009).

Table 2 Best-fitting Parameters for the X-ray Continua

State	$N_{\rm H}$ $(10^{22}\,{\rm cm}^{-2})$	Γ	${\rm Flux}_{2-10{\rm keV}}$ $(10^{-11}\,{\rm erg\,s^{-1}\,cm^{-2}})$	$L_{2-10{\rm keV}}$ $(10^{43}\,{\rm erg\,s^{-1}})$	Cstat/d.o.f.
Combined	0.90 ± 0.04	1.87 ± 0.02	2.41	1.89	2378/2098
ID 3148	0.94 ± 0.06	1.87 ± 0.03	1.97	1.55	2243/2098
ID 3452	0.86 ± 0.05	1.88 ± 0.03	2.89	2.28	2299/2098
Normal	0.89 ± 0.06	1.90 ± 0.03	2.06	1.62	2232/2098
Peak	0.88 ± 0.06	1.83 ± 0.03	2.95	2.32	2287/2098

3.2 Absorption Lines

In order to increase the signal-to-noise ratio, the two observations were first combined in order to perform the detailed analysis. We identified X-ray absorption in helium-like and hydrogen-like neon, magnesium, silicon and L-shell silicon with –400 km s^{-1} compared to the line rest energy in the IRAS 18325–5926 frame, marked in red in Figure 2. Then, we established another set of absorption lines including Mg XI(r) with a Poisson probability of 0.9997 at redshift zero, or with –6000 km s^{-1} with respect to the systemic redshift, marked in green.

The set of lines with -400 km s^{-1} velocity is similar to the absorption features found in Seyfert 1s, which are associated with X-ray WAs, based on the support of previous works (e.g. Netzer et al. 2003; McKernan et al. 2007). Assuming that the lines came from a single WA, they should share the same outflow velocity and the same full width at half maximum (FWHM). We used the two Mg XI lines (Mg XI(r) & Mg XI Lyβ) that are at the same atomic state to constrain the FWHM and then applied it to the seven prominent lines (Si XIV, Si XIII, Si X, Mg XI, Mg XII and Ne X) when fitting Gaussian profiles. Four lines of Si X, Mg XI and Ne X were well fitted with a FWHM

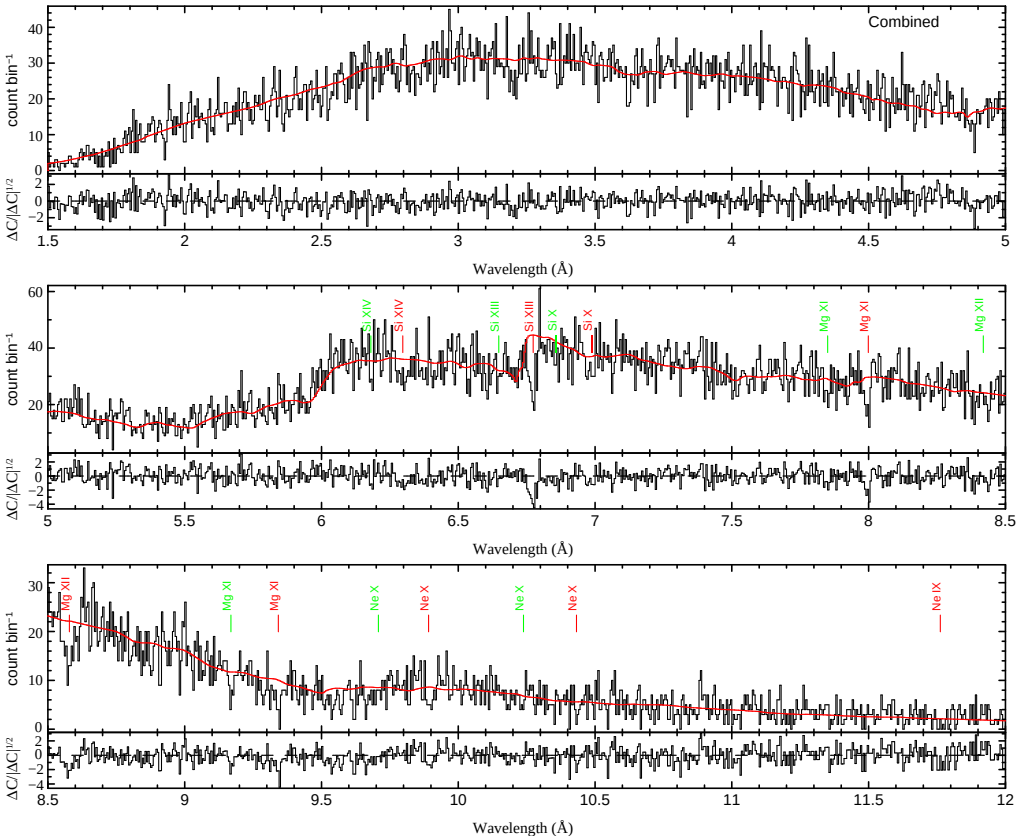

Fig. 2 IRAS 18325–5926's spectra. The intrinsic absorption lines are marked with red, while the absorption lines at zero redshift are marked with green (color online).

of $\sim 600\ \mathrm{km\ s^{-1}}$, but the other three highly ionized ions of Si XIII, Si XIV and Mg XII displayed broader Doppler widths, as shown in the upper panel of Figure 3.

As a consequence, we refitted the seven lines assuming they were from two WA components. The refitting yielded an improvement to the three highly ionized lines ($\Delta C \sim 6$ for 20 d.o.f. for each individual line) compared to the previous result, as shown in the lower panel of Figure 3. These lines are decomposed into narrow and broad components, and the fitting parameters of dominant components are presented in Table 3. The narrow component has a FWHM of $570 \pm 240\ \mathrm{km\ s^{-1}}$ and an outflow velocity of $340 \pm 110\ \mathrm{km\ s^{-1}}$, while the broad component has a FWHM of $1360 \pm 560\ \mathrm{km\ s^{-1}}$ and an outflow velocity of $460 \pm 220\ \mathrm{km\ s^{-1}}$. The comparison between the combined spectrum and the best-fitting model is shown in Figure 4.

Among the line system at zero shift, three more lines with Poisson probability greater than 0.990 other than Mg XI(r) were found at 6.180 Å, 7.850 Å and 8.438 Å, which could be Si XIV, Mg XI Lyβ and Mg XII, respectively. One immediate explanation is Galactic absorption. Near the position of IRAS 18325–5926 ($l = 336°$, $b = -21°$), there is a diffuse zero redshift ionized absorber traced by O VI in the UV band (e.g. Savage et al. 2003). The absorbing gas in the X-ray band may be related to this UV absorber, in the form of high velocity clouds in the Galactic halo (Fox et al. 2006). High temperature would be necessary to produce such highly ionized ions. However, such a highly ionized Galactic absorption has never been reported before.

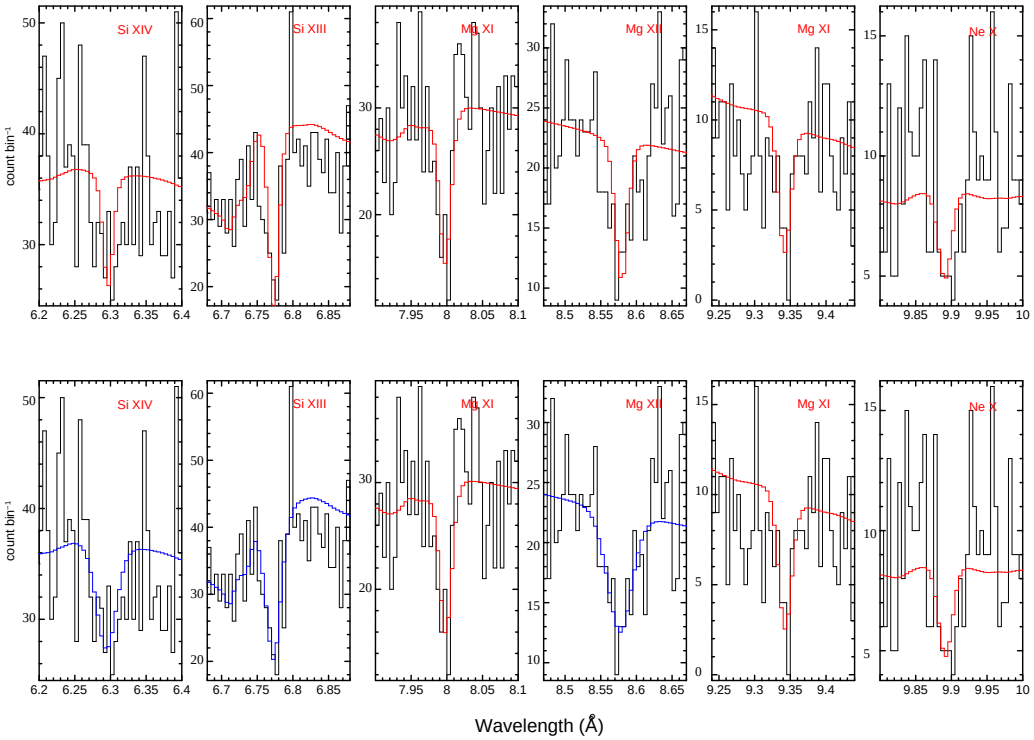

Fig. 3 Comparison between the best-fitting model of absorption lines. The lines in the upper panel are fitted with one set of Gaussian lines, while those in the lower panel are fitted with two sets of Gaussian lines. Three highly ionized ions of Si XIII, Si XIV and Mg XII display broader Doppler width.

Table 3 Intrinsic Absorption Lines in the Combined Spectrum

Ion Name & $\lambda_{\rm rest}$ (Å)	FWHM (km s^{-1})	$\lambda_{\rm obs}$ (Å)	Flux (10^{-6} ph cm^{-2} s^{-1})	EWs (mÅ)
Si XIV Lyα (6.180)	1360	6.295	7.4 ± 3.4	16 ± 7
Si XIII(r) (6.648)	570	6.773	≤ 9.2	≤ 21
	1360	6.771	9.0 ± 6.2	21 ± 14
Si X(r) (6.859)	570	6.988	3.5 ± 2.4	8 ± 6
Mg XI Lyβ (7.850)	570	7.997	8.3 ± 2.5	26 ± 8
Mg XII Lyα (8.421)	1360	8.579	12.7 ± 5.2	47 ± 19
Mg XI(r) (9.169)	570	9.341	13.8 ± 3.8	66 ± 18
Ne X Lyγ (9.708)	570	9.891	8.7 ± 4.8	48 ± 26

Another possible interpretation is a high velocity outflow with 6000 km s^{-1}. The high velocity outflow is not rare in AGNs. Crenshaw et al. (1999) performed a survey of Seyfert galaxies and found that nearly 60% of the targets showed outflow velocities up to 2000 km s^{-1} in the UV band, while in the X-ray band some 30% of AGNs show evidence for an ionized wind of $v \sim 0.1c$, which, however, are associated with Fe XXV and Fe XXVI lines most of the time (Tombesi et al. 2010). We detected the absorption feature at 1.925 Å, which could be Fe XXV with an outflowing velocity of 13 000 km s^{-1}, however, its Poission probability is only 0.995. Since the signal-to-noise ratio of this set of lines is not high enough, we cannot differentiate between these two possibilities.

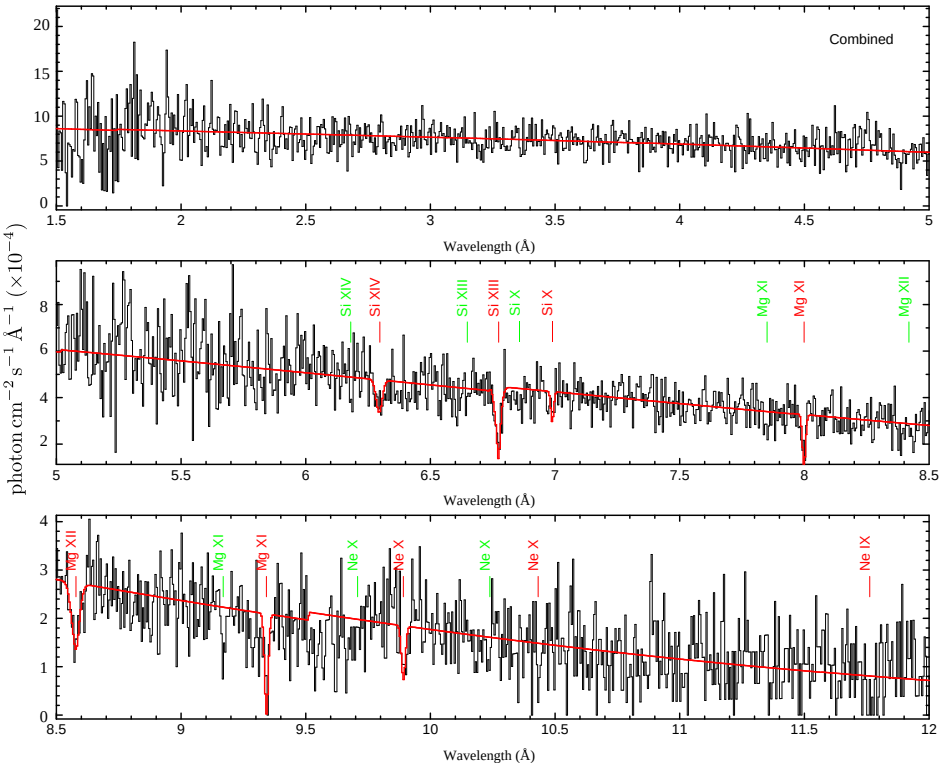

Fig. 4 Comparison between the combined spectrum and the best-fitting model with two sets of Gaussian lines.

There are still some unidentified features. Three absorption features around 3.2 Å, 4.9 Å and 9.5 Å have Poisson probabilities of 0.9978, 0.9989 and 1.000, respectively. The responsible ions could be Ar XVIII, S XV and Fe XX considering the systemic redshift, or these features could be spurious. The emission-like feature at 9.85 Å is unidentified, and has a Poisson probability of 0.0003.

4 PHOTOIONIZATION MODEL FITTING

In Section 3, we identified the most prominent absorption lines. In this section we go further to fit the spectra with WA models. There are good reasons for this. Firstly, the continuum absorption of the WA is not negligible, which is attributed to the neutral absorption in the previous section. Then the contribution from the two WA components can be disentangled. Finally, the very weak lines which are predicted by the model can also help to constrain the spectrum.

4.1 Photoionization Model

The publicly available photoionization code XSTAR [1] is the tool to model the physical conditions of the absorbing gas. We use PVM_XSTAR (Noble et al. 2009) to generate grids of models, and which provide parallel execution of XSTAR 2.1ln11. Default solar abundances (Grevesse et al. 1996) are adopted throughout this work.

[1] *http://heasarc.gsfc.nasa.gov/docs/software/xstar/xstar.html*

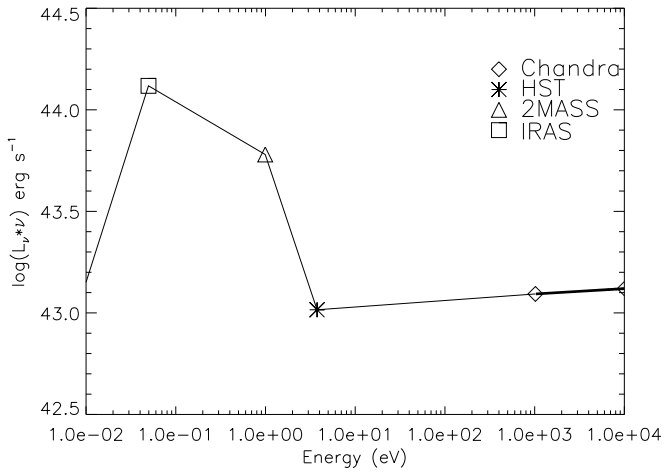

Fig. 5 SED of IRAS 18325–5926. The thick solid line is the intrinsic X-ray spectrum. The radio data point is beyond the left side of the figure.

The observed spectral energy distribution (SED) is used as an input for generating the photoionization models. We constructed the SED of IRAS 18325–5926 by including the intrinsic ionizing X-ray spectrum and obtained some other data from NED: 4.85 GHz radio data from the Parkes-MIT-NRAO southern survey, 25 μm data from IRAS, J band data from 2MASS and F330W data from HST. The flux point at the 1 keV band of the intrinsic X-ray continuum was simply linked to the optical point and to other data in the SED by straight lines in log-log space, as shown in Figure 5. The properties of WA model grids are mainly driven by the X-ray continuum of SED. Removing a prominent IR-optical continuum bump from the SED yielded WA parameters that were within the 90 percent confidence intervals obtained when the bump was not removed (McKernan et al. 2003). The band below IR makes little difference to the ionization balance of WAs (Krolik & Kriss 2001). Thus, our SED is good enough to generate photoionization models for the two WA components with FWHM of 570 and 1360 $\mathrm{km\ s^{-1}}$.

The photoionization model used here contains three parameters: red-shift z; total neutral hydrogen column density N_{H}; and the ionization parameter $\xi = L_{\mathrm{ion}}/(n_{\mathrm{e}}R^2)$, where L_{ion} is the ionizing luminosity in the range 1–1000 Ryd, n_{e} is the electron density and R is the distance from the ionized gas to the central ionizing source. L_{ion} of IRAS 18325–5926 is about $1 \times 10^{44}\ \mathrm{erg\ s^{-1}}$, derived from the SED.

4.2 The Warm Absorbers

We fitted the combined spectrum and the two groups of data with the two photoionization models. The results of our fit are summarized in Table 4.

For the combined spectrum, we show the best fitting model in Figure 6, in which the absorption lines with $-400\,\mathrm{km\ s^{-1}}$ are well represented. The two photoionization WA models applied are displayed in Figure 7, where the broad component contributes more in Si XIV, Si XIII and Mg XII lines but less in Mg XI lines and the narrow component also absorbs the continuum emission. The broad WA is more ionized than the narrow WA and seems to have a higher outflow velocity, although the

Table 4 Best-fitting parameters for the WA components

State	cold $N_{\rm H}$ (10^{22} cm^{-2})	Γ	$N_{\rm H}$ (10^{21} cm^{-2})	$\log\xi$ (erg s cm^{-1})	redshift z	C/d.o.f.	$^{a}\Delta C$
Combined	0.74 ± 0.09	1.94 ± 0.02	6.07 ± 0.60 3.78 ± 1.59	1.58 ± 0.09 2.35 ± 0.25	0.0190 ± 0.0002 0.0184 ± 0.0010	2196/2092	182
ID 3148	0.71 ± 0.07	1.95 ± 0.03	10.26 ± 2.67	≤ 1.72	0.0187 ± 0.0003	2160/2095	83
ID 3452	0.71 ± 0.10	1.95 ± 0.04	$5.72^{+0.25}_{-2.09}$ 4.56 ± 1.92	$1.58^{+0.02}_{-0.27}$ 2.37 ± 0.27	0.0192 ± 0.0003 0.0185 ± 0.0010	2197/2092	102
Normal	$^{b}0.71$	1.95 ± 0.06	7.55 ± 0.98	1.69 ± 0.08	0.0189 ± 0.0002	2207/2093	25
Peak	$^{b}0.71$	1.94 ± 0.03	$5.67^{+0.08}_{-1.12}$ 4.86 ± 2.07	1.41 ± 0.17 2.20 ± 0.22	0.0194 ± 0.0004 0.0178 ± 0.0009	2139/2093	148

Notes: ^{a} Change in the Cash statistics between models with WAs and continuum models. ^{b} The column density is fixed at the value of the first group of data.

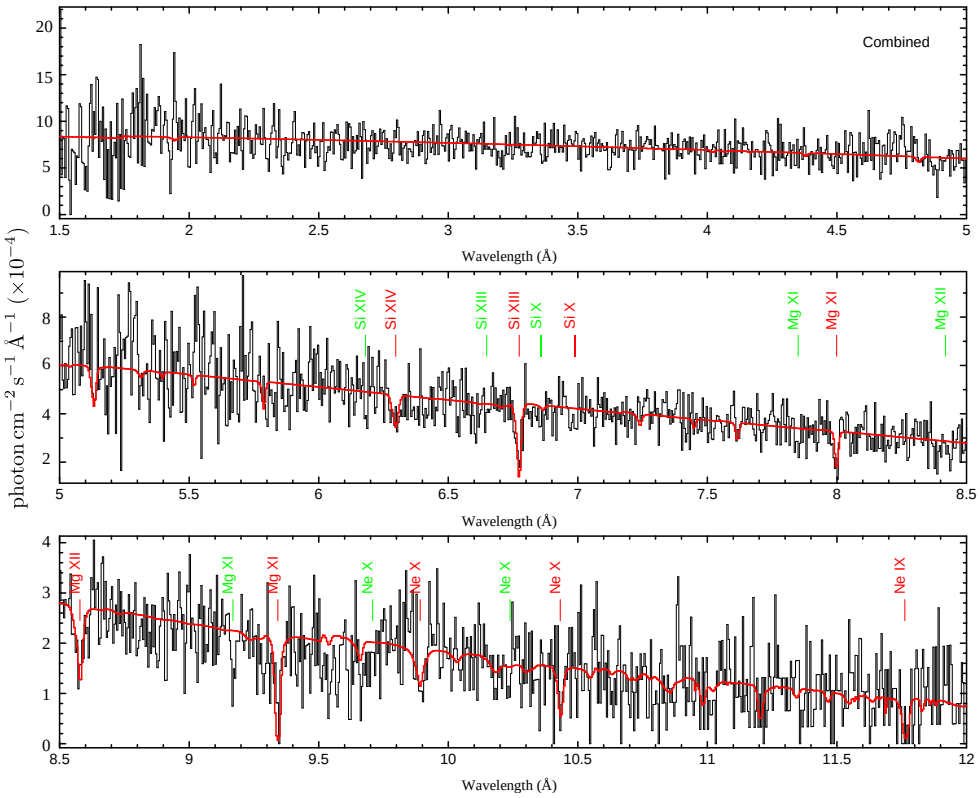

Fig. 6 Combined spectrum fitted with the two WAs. Many weak absorption features are presented.

deviation is within the error tolerance. Using the two photoionization models provides an improvement of $\Delta C = 182$ compared to the continuum fitting.

For the first group of data, we fitted the ID 3148 spectrum with one narrow WA component, but for ID 3452 we used both the narrow and the broad WA components. If we add a broad WA component to ID 3148, its column density would only be a few 10^{20} cm^{-2} and the fitting does not provide any improvements in the statistics. The comparison of the spectra of ID 3148 and 3452

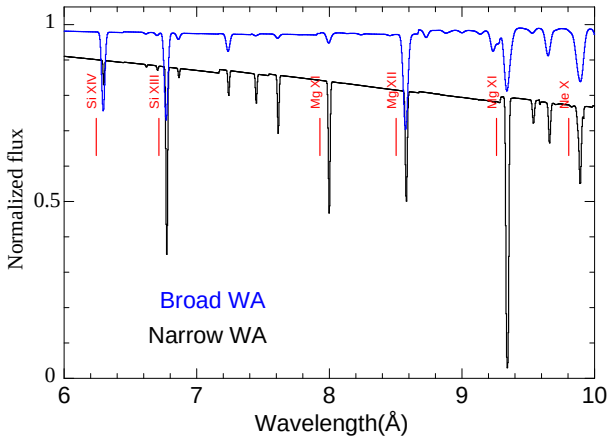

Fig. 7 Two WAs that are used to model the combined spectrum of IRAS 18325–5926 are shown on a scale where 1 is the incident continuum level.

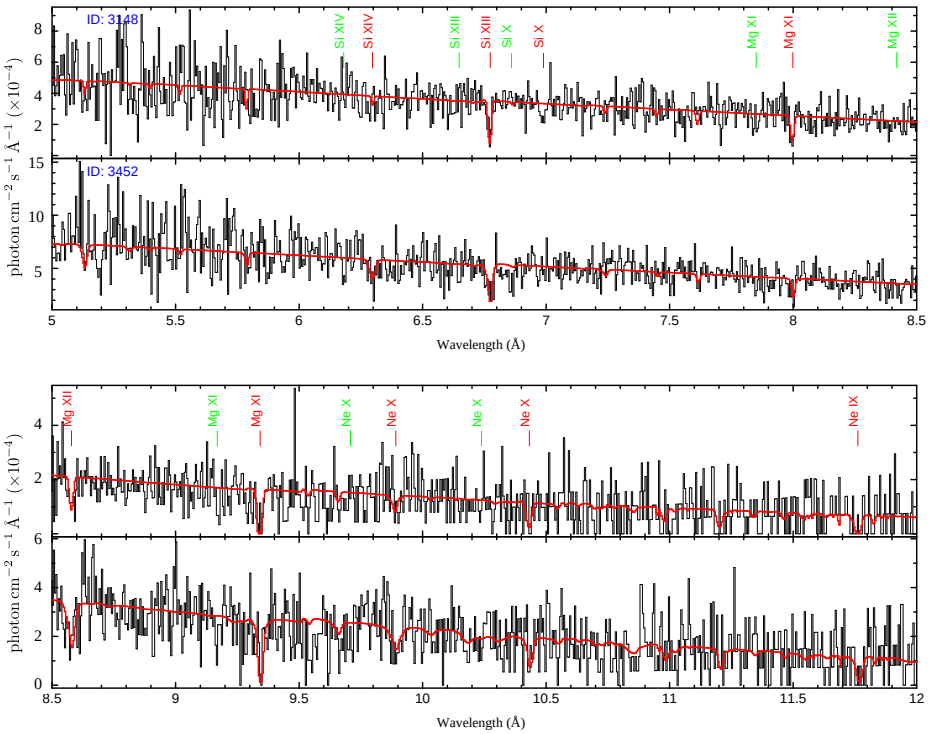

Fig. 8 Comparison of ID 3148 and 3452 spectra fitted with photoionization models. Si XIII, Si XIV and Mg XII are broader in the ID 3452 spectrum than that in the ID 3148.

with their best fitting models is shown in Figure 8. The ID 3148 spectrum has narrower Mg XII and Si XIII lines. The cold gas column density is the same for ID 3148 to 3452, and the ionization parameter and redshift of narrow WA are within the error bars. However, the column density of narrow WA decreased to half from ID 3148 to 3452 and the broad WA appeared during three days.

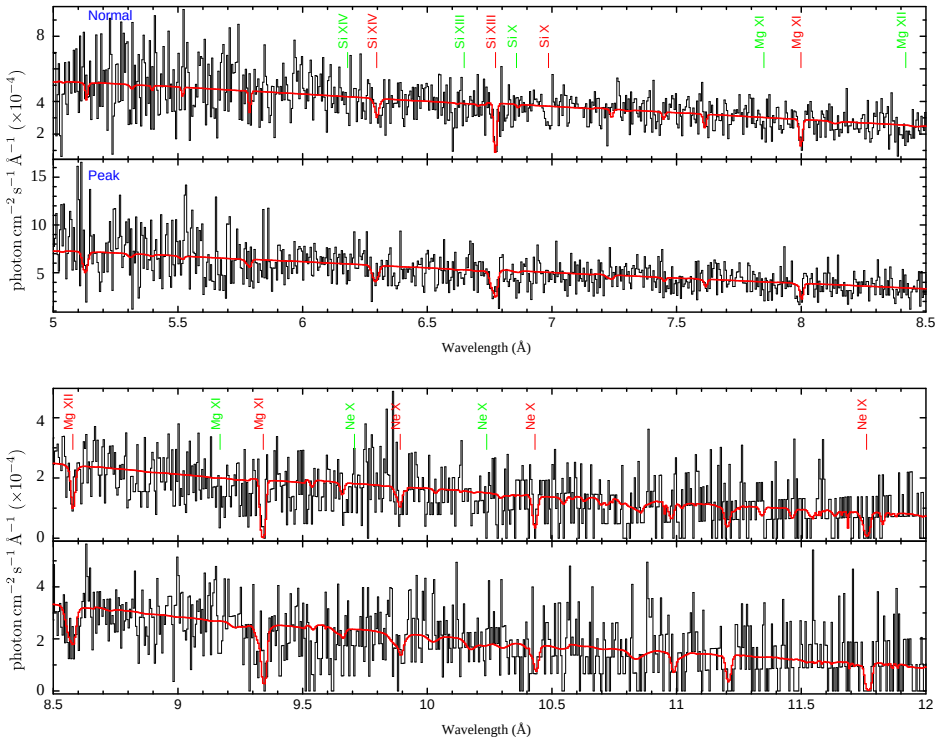

Fig. 9 Comparison of "normal" and "peak" spectra fitted with photoionization models. Si XIII and Mg XII are broader in the "peak" spectrum, while Si X is much more prominent in the "normal" spectrum.

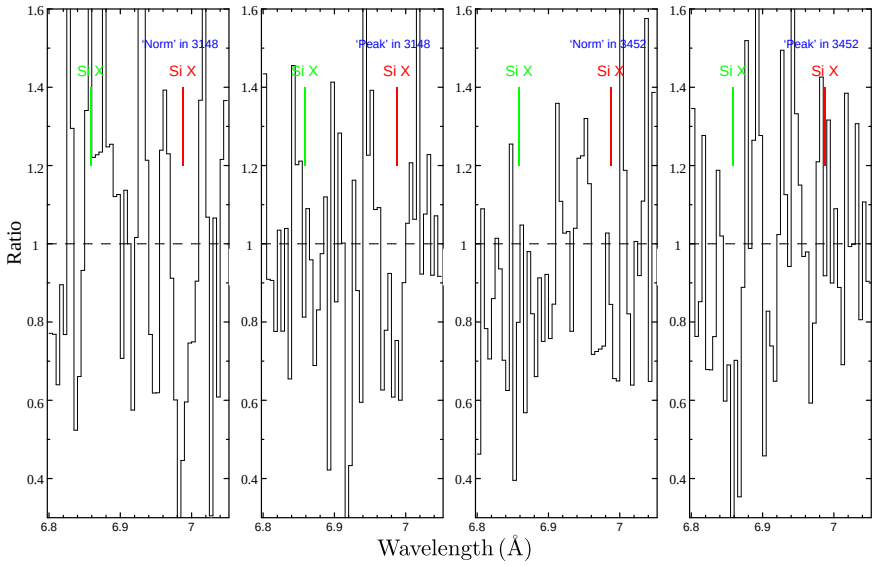

Fig. 10 Si X lines in different time intervals.

For the second group of data, the cold gas column density was generally fixed to $N_{\rm H} = 0.71\,{\rm cm}^{-2}$ obtained from ID 3148 and 3452, which did not vary over three days. Like the first group, the "peak" spectrum contains a broad WA component, but the "normal" spectrum is well fitted with a single narrow WA. Nothing changes significantly for the narrow WA, particularly the outflow velocity.

From the above analysis, the most interesting thing is that much stronger Si X absorption lines are displayed in both the ID 3148 and "normal" spectra. Unfortunately, the Si X absorption line would not be fitted with the photoionization models, because the silicon L-shell lines are omitted from the XSTAR database (McKernan et al. 2007). Thus we did a more detailed estimation for the Si X line along the time sequence, as shown in Figure 10. It changed quickly, responding to the luminosity: strongest to the lowest luminosity ("normal" in ID 3148) but nearly disappeared to the highest luminosity ("peak" in ID 3452). The zero redshift Si X absorption line also seems to change with luminosity, getting stronger from low luminosity to high luminosity. If this is confirmed, this set of lines would be determined to be a high velocity outflow.

5 DISCUSSION

5.1 The Location of WAs

The periodicity of IRAS 18325–5926 did not affect the WAs in a direct way. There are no significant changes in the velocities between "normal" and "peak" states. The existence of the broad WA in a "peak" state is mainly due to its existence in ID 3452. As a consequence, the possibility that a broad WA component is orbiting the BH is ruled out.

The large error bars in the ionization parameters of the narrow WA prevent us from detecting the response of WA to the ionizing luminosity. However, the quick response in opacity of Si X, which is ionized to a lower degree and thought to be associated with the narrow WA, indicates an electronic density larger than $5 \times 10^7\,{\rm cm}^{-3}$ (Nicastro et al. 1999). Combined with the luminosity and the ionization parameter, the distance of the narrow WA from the BH should be smaller than 0.07 pc.

We estimated the distance of the BLR to the BH to be about 0.002 pc, using $r_{\rm BLR} \propto L_{\rm Bol,44}^{0.5}$ light days (Wandel et al. 1999). The distance of the inner edge of the torus to the BH is about 1 pc, determined by $1 \times L_{\rm ion,44}^{0.5}$ pc (Krolik & Kriss 2001). Considering $\xi = L_{\rm ion}/(n_{\rm e}R^2)$, for the BLR and the torus, the electron density would be $2.5 \times 10^9\,{\rm cm}^{-3}$ and $5 \times 10^4\,{\rm cm}^{-3}$, respectively. Since the column density of the broad WA is $5 \times 10^{21}\,{\rm cm}^{-2}$, the thickness of the clouds should be 1×10^{-7} pc at BLR or 0.03 pc at torus. A cloud near the torus with a thickness of 0.03 pc, moving in and covering our line of sight to the ionizing source over three days, seems counterintuitive.

As a consequence, combined with the constraint on distance by Si X, the location of the WA is more likely to be near the BLR or accretion disk. The broad WA that may be a several-million-km-thick cloud which moved into our line of sight, while half of the narrow WA moved out due to the decrease of the column density.

5.2 The Origin of WAs

Based on the *ASCA* and *RXTE* observations during 1997–1998, $4 \sim 5$ years before the *Chandra* observations, Iwasawa et al. (2004) found that IRAS 18325–5926 had a steep continuum slope $\Gamma \sim 2.2$, a prominent Fe XXV emission line (1.859 Å) and S XVI radiative recombination continua (RRC, 3.548 Å). The authors suggested that these features were caused by the reflection from a highly ionized disk. However, neither of the emission features can be detected in the *Chandra* observations and the spectral slope is flatter than that in early observations. The reflection state was dissolved during the *Chandra* observations in 2002.

It is interesting to consider where the highly ionized gas on the disk has gone. If the gas traveled with a velocity of 400 km ${\rm s}^{-1}$ along our line of sight in the $4 \sim 5$ years, it would reach a projected

distance of 0.002 pc. Its real distance to the BH is larger than or equal to 0.002 pc, which is quite coincident with the distance of WAs. In addition, the adjacent gas regions in the ionized disk may have dramatically different densities and temperatures (Nayakshin et al. 2000). The large jump in temperature of the adjacent gas can naturally explain the narrow and broad WAs. The gas with FWHM of $570\ \mathrm{km\ s^{-1}}$ is followed by gas with FWHM of $1360\ \mathrm{km\ s^{-1}}$, appearing as narrow and broad WAs. When the narrow WA gradually passed our line of sight, the following broad WA moved in. As a result, the origin of the WAs should be the ionized wind from the accretion disk.

Since IRAS 18325–5926 is a Seyfert 2 galaxy, we are more likely to see through the vertical part of the funnel-shaped thin shell outflow (Elvis 2000). In the vertical part, the transverse velocity is large, which is the reason for the quick change of the narrow WA to the broad WA. Considering the highly ionized gas to be the predecessor of the WAs, we predict that there are seldom WAs in IRAS 18325–5926 this year.

6 CONCLUSIONS

We draw a brief conclusion here. We analyzed *Chandra* HETGS spectra of IRAS 18325–5926 and reported warm absorbers with high energy resolution in a Seyfert 2 galaxy for the first time. An intrinsic absorbing line system with an outflow velocity $\sim 400\ \mathrm{km\ s^{-1}}$ was generated by two warm absorbers, the FWHM of which are $570\ \mathrm{km\ s^{-1}}$ and $1360\ \mathrm{km\ s^{-1}}$, respectively. The broad WA is only found in the ID 3452 observation and the column density of narrow WA decreased to half from ID 3148 to 3452. Thus, we believe that the two WAs were adjacent and moving transversely across our line of sight. We constrained the distance of the absorbers to a small value and suggested that the absorbers came from the highly ionized accretion disk wind ejected five years ago. The perspective of this type 2 Seyfert provides the best situation from which to investigate the vertical part of the funnel-like outflows. Meanwhile, the periodicity of IRAS 18325–5926 did not show any influence on the WAs at all. Another set of possible zero redshift absorbing line systems was also detected. It could be due to Galactic absorption with very high temperature or an intrinsic outflow with very high velocity $\sim 6000\ \mathrm{km\ s^{-1}}$.

Acknowledgements The authors gratefully acknowledge the anonymous referee for their insights and comments that improved this paper. The authors would also like to thank the support of the *Chandra* X-ray center. Support for this work was provided by the Program for New Century Excellent Talents in University (NCET), the National Natural Science Foundation of China (Grant Nos. 10878010, 10221001 and 10633040) and the National Basic Research Program of China (Grant No. 2007CB815405).

References

Canizares, C. R., Davis, J. E., Dewey, D., et al. 2005, PASP, 117, 1144
Cash, W. 1976, A&A, 52, 307
Comastri, A., Vignali, C., Cappi, M., et al. 1998, MNRAS, 295, 443
Crenshaw, D. M., Kraemer, S. B., Boggess, A., et al. 1999, ApJ, 516, 750
Elvis, M. 2000, ApJ, 545, 63
Fabian, A. C., Lee, J. C., Brandt, W. N., et al. 1998, arXiv:astro-ph/9803075
Fox, A. J., Savage, B. D., & Wakker, B. P. 2006, ApJS, 165, 229
Ganguly, R., & Brotherton, M. S. 2008, ApJ, 672, 102
George, I. M., Turner, T. J., Netzer, H., et al. 1998, ApJS, 114, 73
Grevesse, N., Noels, A., & Sauval, A. J. 1996, in Astronomical Society of the Pacific Conference Series 99, Cosmic Abundances, eds. S. S. Holt, & G. Sonneborn, 117
Halpern, J. P. 1984, ApJ, 281, 90

Houck, J. C. 2002, High Resolution X-ray Spectroscopy with XMM-Newton and Chandra (*http://adsabs. harvard.edu/abs/2002hrxs.confE..17H*)
Iwasawa, K., Fabian, A. C., Brandt, W. N., et al. 1998, MNRAS, 295, L20
Iwasawa, K., Lee, J. C., Young, A. J., Reynolds, C. S., & Fabian, A. C. 2004, MNRAS, 347, 411
Jones, D. H., Saunders, W., Colless, M., et al. 2004, MNRAS, 355, 747
Kalberla, P. M. W., Burton, W. B., Hartmann, D., et al. 2005, A&A, 440, 775
Kinkhabwala, A., Sako, M., Behar, E., et al. 2002, ApJ, 575, 732
Komossa, S., & Fink, H. 1997, A&A, 327, 555
Krolik, J. H., & Kriss, G. A. 2001, ApJ, 561, 684
Krongold, Y., Nicastro, F., Brickhouse, N. S., Elvis, M., & Mathur, S. 2005, ApJ, 622, 842
Krongold, Y., Nicastro, F., Elvis, M., et al. 2007, ApJ, 659, 1022
Matt, G., Bianchi, S., Awaki, H., et al. 2009, A&A, 496, 653
Matt, G., Bianchi, S., D'Ammando, F., & Martocchia, A. 2004, A&A, 421, 473
McKernan, B., Yaqoob, T., George, I. M., & Turner, T. J. 2003, ApJ, 593, 142
McKernan, B., Yaqoob, T., & Reynolds, C. S. 2007, MNRAS, 379, 1359
Misawa, T., Charlton, J. C., Eracleous, M., et al. 2007, ApJS, 171, 1
Nayakshin, S., Kazanas, D., & Kallman, T. R. 2000, in American Institute of Physics Conference Series 510, eds. M. L. McConnell, & J. M. Ryan, 250
Netzer, H., Kaspi, S., Behar, E., et al. 2003, ApJ, 599, 933
Nicastro, F., Fiore, F., Perola, G. C., & Elvis, M. 1999, ApJ, 512, 184
Noble, M. S., Ji, L., Young, A., & Lee, J. C. 2009, in Astronomical Society of the Pacific Conference Series 411, Astronomical Data Analysis Software and Systems XVIII, eds. D. A. Bohlender, D. Durand, & P. Dowler, 301
Piconcelli, E., Jimenez-Bailón, E., Guainazzi, M., et al. 2005, A&A, 432, 15
Pounds, K. A., & Vaughan, S. 2011, MNRAS, 413, 1251
Reynolds, C. S. 1997, MNRAS, 286, 513
Risaliti, G., & Elvis, M. 2010, A&A, 516, A89
Risaliti, G., Elvis, M., & Nicastro, F. 2002, ApJ, 571, 234
Sako, M., Kinkhabwala, A., Kahn, S. M., et al. 2002, in X-ray Spectroscopy of AGN with Chandra and XMM-Newton, eds. T. Boller, S. Komossa, S. Kahn, H. Kunieda, & L. Gallo, 191
Savage, B. D., Sembach, K. R., Wakker, B. P., et al. 2003, ApJS, 146, 125
Steenbrugge, K. C., Fenovčík, M., Kaastra, J. S., Costantini, E., & Verbunt, F. 2009, A&A, 496, 107
Tombesi, F., Cappi, M., Reeves, J. N., et al. 2010, A&A, 521, A57
Wandel, A., Peterson, B. M., & Malkan, M. A. 1999, ApJ, 526, 579
Zhang, S. N., Ji, L., Marshall, H. L., et al. 2011, MNRAS, 410, 2274